Morphological Changes of Carbides During Creep and Their Effects on the Creep Properties of Inconel 617 at 1000 °C

SHIGEMITSU KIHARA, JOHN B. NEWKIRK, AKIRA OHTOMO, AND YOSHINORI SAIGA

Creep tests have been correlated with microstructural changes which occurred during creep of Inconel 617 at 1000 °C, 24.5 MPa. The following results were obtained: 1) Fine intragranular carbides which are precipitated during creep are effective in lowering the creep rate during the early stages of the creep regime (within 300 h). 2) Grain boundary carbides migrate from grain boundaries that are under compressive stress to grain boundaries that are under tensile stress. This is explained in terms of[1] the dissolution of relatively unstable carbides on the compressive boundaries,[2] the diffusion of the solute atoms to the tensile boundaries and[3] the reprecipitation of the carbides at the tensile boundaries. The rate of grain boundary carbide migration depends on grain size. 3) $M_{23}C_6$ type carbides, having high chromium content, and M_6C type carbides, having high molybdenum content, co-exist on the grain boundaries. $M_{23}C_6$ type carbides, however, are quantitatively predominant. Furthermore, M_6C occurs less frequently on the tensile boundaries than on the stress free grain boundaries. This is attributed to the difference of the diffusion coefficients of chromium and molybdenum. 4) The grain boundaries on which the carbides have dissolved start to migrate in the steady state creep region. The creep rate gradually increases with the occurrence of grain boundary migration. 5) The steady state creep rate depends not so much on the morphological changes of carbides as on the grain size of the matrix.

INCONEL 617 is a superalloy having excellent creep-rupture strength at high temperatures. It is expected to find wide use for service involving high stress at temperatures around 1000 °C. For example, the alloy is scheduled for use in the tube material of the intermediate heat-exchanger of the high temperature gas cooled reactor (HTGR) for the direct steel making plant which is now being developed as a major national project in Japan.[1] This part, designated IHX, will operate at approximately 1000 °C under a stress of less than 9.8 MPa (1 kg/mm^2).

Many parts of the reactor which operate at high temperatures, like the IHX, are designed on the basis of 100,000 h creep-rupture strength of the materials.[2] But actual 100,000 h creep strength test data are difficult to obtain because the test is too long to be practical. Therefore, this value is usually estimated. When this is done, the changes of microstructure during the actual service at high temperatures should be taken into account. Thus it is important to study the relationship between the creep deformation mechanism and the microstructural changes so that a logical method for the estimation of the long-term creep strength can be achieved. For example, the recent development of the deformation mechanism map for AISI type 304 stainless steel, illustrating the active creep deformation mechanism and the interaction of precipitation particles with dislocations as functions of temperature and stress,[3] will provide much useful information for the logical estimation of its long-term creep strength. It was the purpose of this study to make similar observations for Inconel 617 so that safe designs can be made of high temperature equipment like the IHX.

Inconel 617 is a solid-solution strengthened alloy. However, it has been reported that many compounds, including $M_{23}C_6$, M_6C and MC types of carbides and CrMo(C,N), $\gamma'(Ni_3Al)$ and TiN, are precipitated during exposure at high temperatures.[4,5] The major phases are $M_{23}C_6$ and M_6C types of carbides. These are precipitated both in grain boundaries and as intragranular particles. Other precipitates are rarely formed at 1000 °C. Furthermore, it has been reported that the creep strength of this alloy in 99.9 pct He at 1000 °C is remarkably reduced by surface decarburization.[6,7] Therefore it is expected that carbides are associated with the creep strength of Inconel 617 at 1000 °C, as Mankins[4] *et al* indicated. In support of this idea Mino *et al*[8] reported the occurrence of grain boundary migration during creep of Inconel 617 at 1000 °C and suggested that grain boundary carbides act to suppress grain boundary migration, which is one of the recovery mechanisms. However, the morphological changes of carbides during creep have not been extensively studied until now.

The work reported here was done to clarify the creep deformation mechanisms and the morphological changes of carbides during creep in Inconel 617. An attempt is made to develop a creep deformation mechanism diagram for this alloy.

SHIGEMITSU KIHARA, AKIRA OHTOMO, and YOSHINORI SAIGA are Research Engineer, Deputy Manager, and Associate Director, respectively, in the Metallurgy Department, Research Institute, Ishikawajima-Harima Heavy Industries Co., Ltd., Tokyo, Japan. JOHN B. NEWKIRK is Professor, Department of Chemistry, University of Denver (Colorado Seminary), Denver, CO 80208.

Manuscript submitted April 3, 1978.

EXPERIMENTAL PROCEDURE

1. Samples Supplied

Three bars, 25mm, 19 mm and 16 mm diameters, of Inconel 617 were supplied by Huntington Alloys, Inc. The chemical compositions of the three bars are shown in Table I. Notice that the chemical compositions of the three bars are almost identical. Their microstructures and the grain sizes, however, are different, probably due to differences in fabricating conditions, forging ratios and temperatures, heat treatment temperatures and durations and so on. To clarify the roles of intragranuar and grain boundary carbides for the creep properties of this alloy, the morphologies of carbides and the grain sizes were varied by the heat treatments shown in Table II. "A" series samples were solution treated and "B" series samples were solution treated, then aged.

2. Creep Tests

Nine samples, treated as shown in Table II, were supplied for the creep tests at 1000 °C under a stress of 24.5 MPa (2.5 kg/mm^2). The dimensions of the creep test specimen are shown in Fig. 1. The creep tests for all samples, except for Bar 1 decarburized (1-C), were done in air. The creep test for 1-C was done under vacuum to keep the specimen from nitriding.

3. Metallography

Observations of microstructures of the samples before the creep tests, during creep and after aging without load were done by optical microscopy, scanning electron microscopy (SEM) and electron probe microanalysis (EPMA). The polished surfaces of the samples were immersion-etched at room temperature for 10 s for optical microscopy and EPMA observations and for 30 min for scanning electron microscope observation. The etchant was Kalling's reagent (5g $CuCl_2$ + 100 cm^3 HCl + 100 cm^3 C_2H_5OH).

RESULTS AND DISCUSSION

1. Microstructures

Continuous grain boundary carbides were present in all three bars as received. Moderately large intragranular carbides existed in Bar 2 as received, although no intragranular carbide was observed in Bars 1 and 3 as received.

Bar 2 was solution treated at 1177 °C to dissolve intragranular carbides without inducing grain growth (2-A). Bars 2 and 3 were solution treated at 1200 °C for 20 h to increase the grain sizes and to dissolve all carbides (3-A and 4-A). The 1000 °C aging treatment for 1000 h was done for all solution treated samples to eliminate the precipitation of carbides during creep (1-B, 3-B and 4-B). Figure 2 shows typical microstructures of the samples after 1 h aging at 1000 °C. Notice the copious precipitation of fine intragranular transition carbides in the "A" series and practically none in the "B" series. This indicates that fine intragranular transition carbides precipitate at first at 1000 °C, and that these compounds dissolve with time at 1000 °C in favor of the growth of the more stable grain boundary carbides.

Figure 3 shows the morphological changes of the carbides in material 1-A with increasing aging time at 1000 °C. Here it is seen that fine intragranular carbides which are probably metastable phases, are quickly precipitated. Later the more massive and stable grain boundary carbides grow, with the concurrent dissolution of the fine intragranular carbides. The intragranular carbides are almost completely gone by 1000 h. Specimens 2-A, 3-A and 4-A showed almost the same metallographic changes of carbides as shown in Fig. 3.

Takahashi *et al*[9] have confirmed that the $M_{23}C_6$ type carbide, whose composition is $Cr_{15.04}$ $Mo_{2.46}$ $Ni_{4.25}$ $Co_{1.19}$ $Fe_{0.06}$ C_6, and the M_6C tpe carbide, whose composition is $Mo_{2.26}$ $Cr_{1.30}$ $Ni_{1.9}$ $Co_{0.52}$ $F_{0.03}$ C coexist at grain boundaries of Inconel 617 when aged at 1000 °C. Figure 4 shows an EPMA of grain boundary carbides in

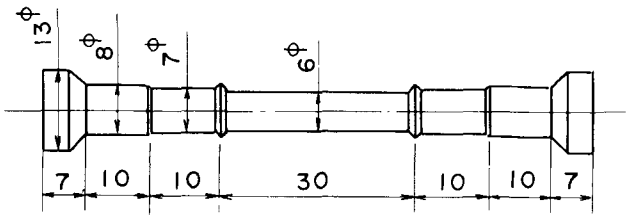

Fig. 1—The dimensions of the creep test specimens. Numbers are in millimeters.

Table I. The Chemical Compositions in Wt Pct and Grain Sizes of the Three Bars of Inconel 617 that were Studied

Element \ Designation	Bar 1	Bar 2	Bar 3
Chromium	22.27	21.98	22.14
Cobalt	12.61	12.14	12.50
Molybdenum	9.07	9.00	9.09
Aluminum	1.05	0.96	1.21
Titanium	0.36	0.40	0.27
Carbon	0.074	0.069	0.065
Nitrogen	0.012	0.047	0.041
Nickel	Bal.	Bal.	Bal.
Grainsize of the bars as received (mm)	0.14	0.11	0.17

Table II. The Treated Conditions, Symbols and Grain Sizes of Samples Supplied for CreepTests

Symbol	Treated condition	Grain Size (mm)
1-A	Bar 1 as received (Solution treated in shop)	O.14
1-B	Bar 1 aged at 1000 °C for 1000 hr	0.14
1-C	Bar 1 decarburized at 1100 °C for 50 hr in He gas of 99.99% (The carbon content is less than 0.01%)	0.18
2-A	Bar 2 quenched after 2 hr at 1177 °C	0.11
2-B	Bar 2 as received (Partially aged in shop)	0.11
3-A	Bar 2 quenched after 20 hr at 1200 °C	0.19
3-B	3-A aged at 1000 °C for 1000 hr	0.19
4-A	Bar 3 quenched after 20 hr at 1200 °C	0.36
4-B	4-A aged at 1000 °C for 1000 hr	0.36

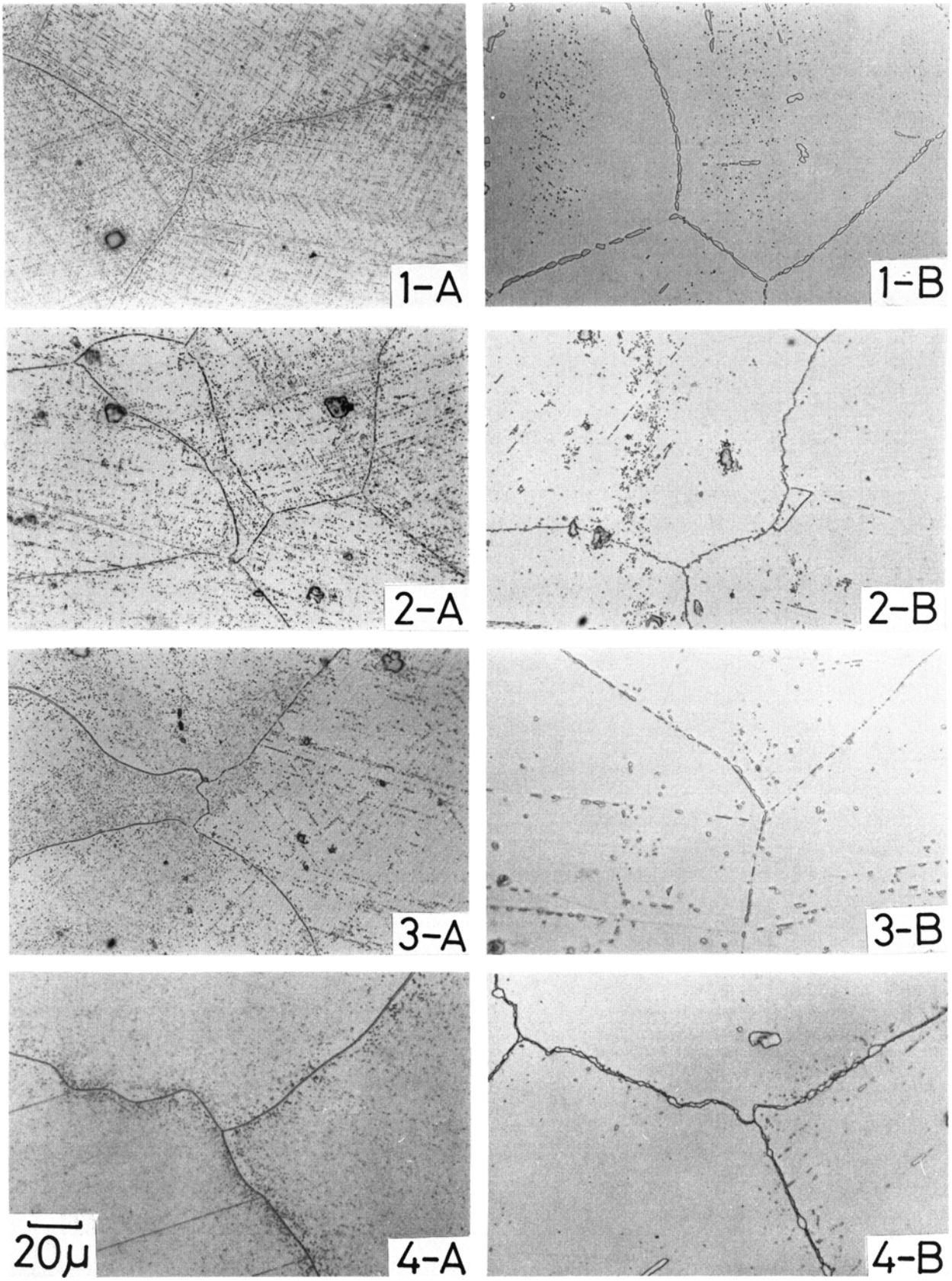

Fig. 2—The microstructures of samples after solution treating and aging for 1 h at 1000 °C show that fine intragranular transition carbides precipitate during early stages of aging ("A" series). The "B" series samples were solution treated and aged for 1000 h at 1000 °C before this 1 h aging at 1000 °C. The resolution of the fine intragranular transition precipitates and the growth of the massive grain boundary carbides are evident.

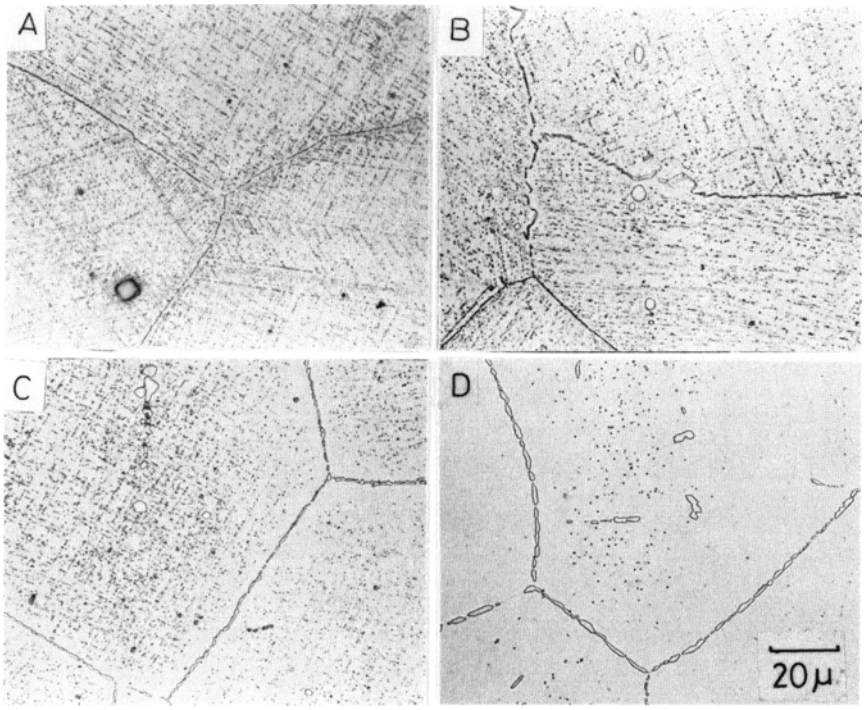

Fig. 3—Typical carbide ripening, observed in specimen 1-A during 1000 °C aging for (*a*) 1 h, (*b*) 10 h, (*c*) 100 h, (*d*) 1000 h, shows that the fine intragranular carbides decrease in number as the grain-boundary carbides grow and finally disappear within 1000 h.

specimen 1-B, which was aged at 1000 °C for 1000 h. Notice that the bright and massive particles in the backscattered electron image of Fig. 4A have high molybdenum and comparatively low chromium contents and the dark and small particles have high chromium and low molybdenum contents. Therefore, it is presumed that the bright and massive particles are M_6C type carbides and the dark and small ones are $M_{23}C_6$ type carbides. The M_6C type carbides, however, are more apt to be localized on the grain boundaries than are the $M_{23}C_6$ type carbides.

2. Creep Tests

The creep curves of nine samples at 1000 °C under a stress of 24.5 MPa are shown in Fig. 5 for similar grain size samples. Figure 6 shows the log of the creep rate plotted against creep time. Here it is seen that the carbide-free 1-C specimen has a much higher creep rate and a shorter creep-rupture life than any of the undecarburized samples. Specimens 1-A, 2-A and 3-A show inverse transient type creep curves, *i.e.*, an initial low in creep rate followed by increase, whereas 1-B and 2-B show linear type creep curves. Specimens 3-B, 4-A and 4-B show normal type creep curves. All this suggests that the creep curves of these samples depend on the heat treatment given to the specimens prior to the creep test. The main difference of microstructure produced by the various heat treatments is the existence of fine intragranular carbides precipitated during creep as shown in Fig. 2. In Fig. 7 the ratios of the creep rates of the "B" series sample (solution treated and aged) to those of the "A" series samples (solution treated only) are plotted against creep time for each part of similar grain size samples. As mentioned before, fine intragranular carbides precipitate during creep in the "A" series samples, while no fine intragranular carbide precipitate during creep in the "B" series samples. Notice that the creep rates of the samples in which fine intragranular carbides precipitate are initially low, but eventually approach those of the samples in which no fine intragranular carbides precipitate. It suggests that the fine intragranular carbides contribute to the lower creep rate in early stages probably by impeding dislocation movement.

Furthermore, Figs. 5, 6, and 7 suggest that the creep curves of all samples except 1-C reach steady state within 300 h and that the rates depend on the grain sizes. The grain size dependence of the steady state creep rate is shown in Fig. 8. Notice that plots for both the solution treated and aged samples lie within the same experimental scatter band. Therefore, we conclude that the fine intragranular carbides can not contribute to the lower creep rate in the steady state region, probably because they decrease in number too much to significantly impede dislocation movement prior to the onset of the steady state creep. In other words, the main contribution of carbon to the creep strength in the steady state region is made not as an intragranular carbide but as interstitial atoms and/or grain boundary carbides.

Figure 9 shows the grain size dependence of the creep rupture life. Notice that the creep rupture lives for the smaller grain size samples are affected by the prior heat treatment conditions. The creep rupture lives for the smaller grain size samples are remarkably decreased by aging before the creep tests. This suggests that the transient creep regions, in which the fine intragranular carbides have an influence, are relatively longer for samples which have shorter creep rupture lives than for those having longer creep rupture lives.

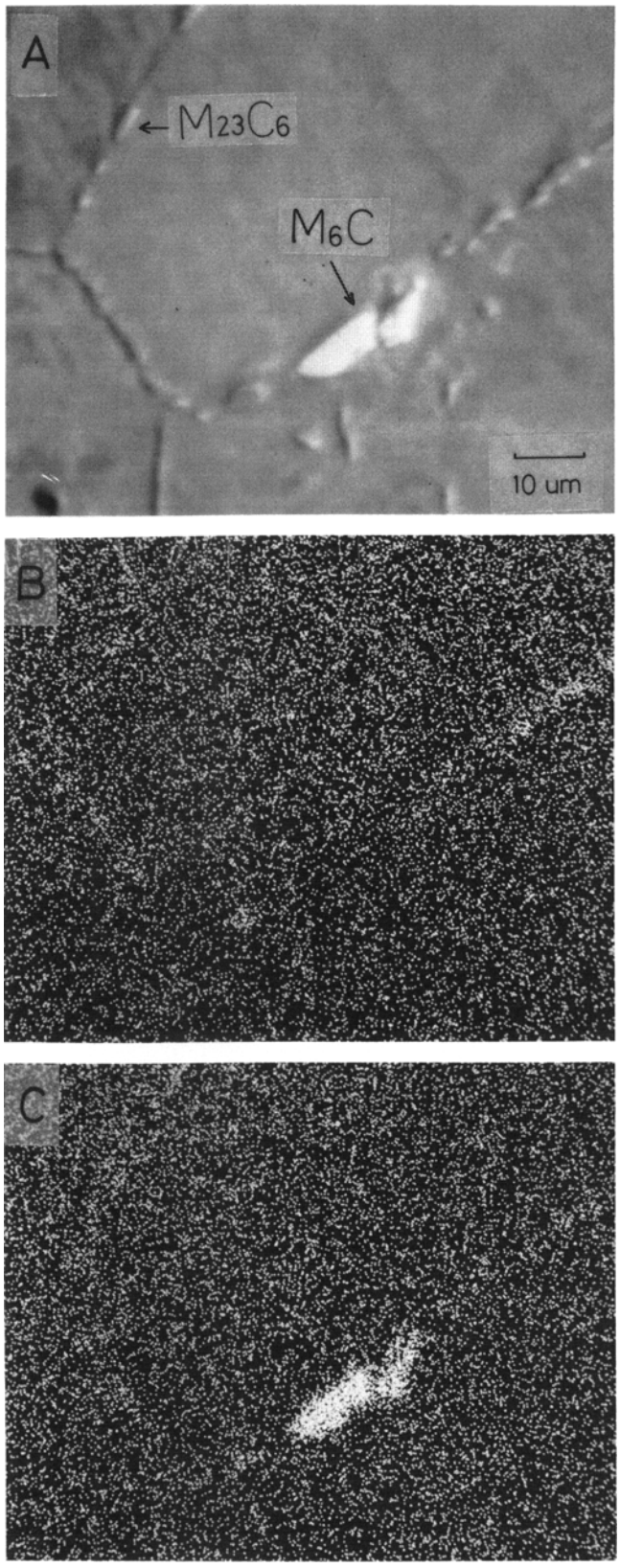

Fig. 4—Elemental X-ray images for grain boundary carbides of 1-B which was aged at 1000 °C for 1000 h. (*a*) Backscattered electron image, (*b*) Cr-Kα and (*c*) Mo-Kα. The bright and massive particles in photo A are M_6C type carbides rich in molybdenum and the dark and small particles are $M_{23}C_6$ type carbides which are rich in chromium.

3. Microstructural Changes during Creep

The microstructural change for each sample during creep at 1000 °C and 24.5 MPa was observed in longitudinal sections of the samples which were creep tested.

3.1 Grain Boundary Migration in Specimen 1-C. Typical microstructural changes for the carbide free specimen 1-C during creep are shown in Fig. 10. Notice that the grain boundaries after 8 h of creep are wavy, as shown in Fig. 10A. This is attributed to grain boundary migration which occurred during the creep deformation.[10] Grain boundary migration was observed at all grain boundaries regardless of the stress direction. Occasionally cracks occurred on grain boundaries perpendicular to the tensile axis as shown in Fig. 10B.

3.2 Migration of Grain Boundary Carbides. The microstructural changes found in specimen 2-B after 100 h and 338 h of tensile creep to plastic strains of 2 and 6 pct are shown in Fig. 11A and B, respectively. Notice that the morphologies of the carbides are not the same at all grain boundaries after 100 h of creep. There exist many carbides on the grain boundaries which are oriented normal to, or at high angles to the tensile stress axis and few carbides on the grain boundaries which are oriented parallel to, or at low angles to the tensile stress axis. This phenomenon is clearly observed in Fig. 11B, where the sample was creep tested for 388 h.

Another interesting result is that the grain boundaries on which no carbides exist are wavy in specimen 2-B as well as 1-C. This suggests that grain boundary migration also occurred on those grain boundaries of 2-B. Grain boundary migration occurring between discrete precipitated particles has also been observed during creep in AISI type 316 stainless steel by Garofalo *et al.*[11]

Compressive creep tests for specimen 2-B were also done at 1000 °C and 24.5 MPa to confirm and clarify the effect of stress direction on the preferred formation of carbides at certain grain boundaries. Similar to the tensile creep test, the changes of microstructures caused by 100 h and 388 h of compressive creep are shown in Fig. 12A and B, respectively. Here it is seen that carbides form preferentially on grain boundaries which are parallel to the compressive stress axis and dissolve on grain boundaries which are normal to the compressive stress axis. The results of these tensile and compressive creep tests suggest that carbides are thermodynamically more stable on grain boundaries which are under tensile stress than on grain boundaries which are under compressive stress.

This phenomenon was observed in all the samples that were creep-tested. The carbides on the tensile boundaries grew rapidly and those on the compressive boundaries disappeared even in the aged samples, 1-B, 2-B, 3-B and 4-B, in which no carbides precipitated during creep. This suggests that the phenomenon is not the preferential precipitation of carbides on the tensile boundary, but the migration of carbides from the compressive boundary to the tensile boundary. The migration of carbides is understandable as a sequence containing the dissolution of carbides at the compres-

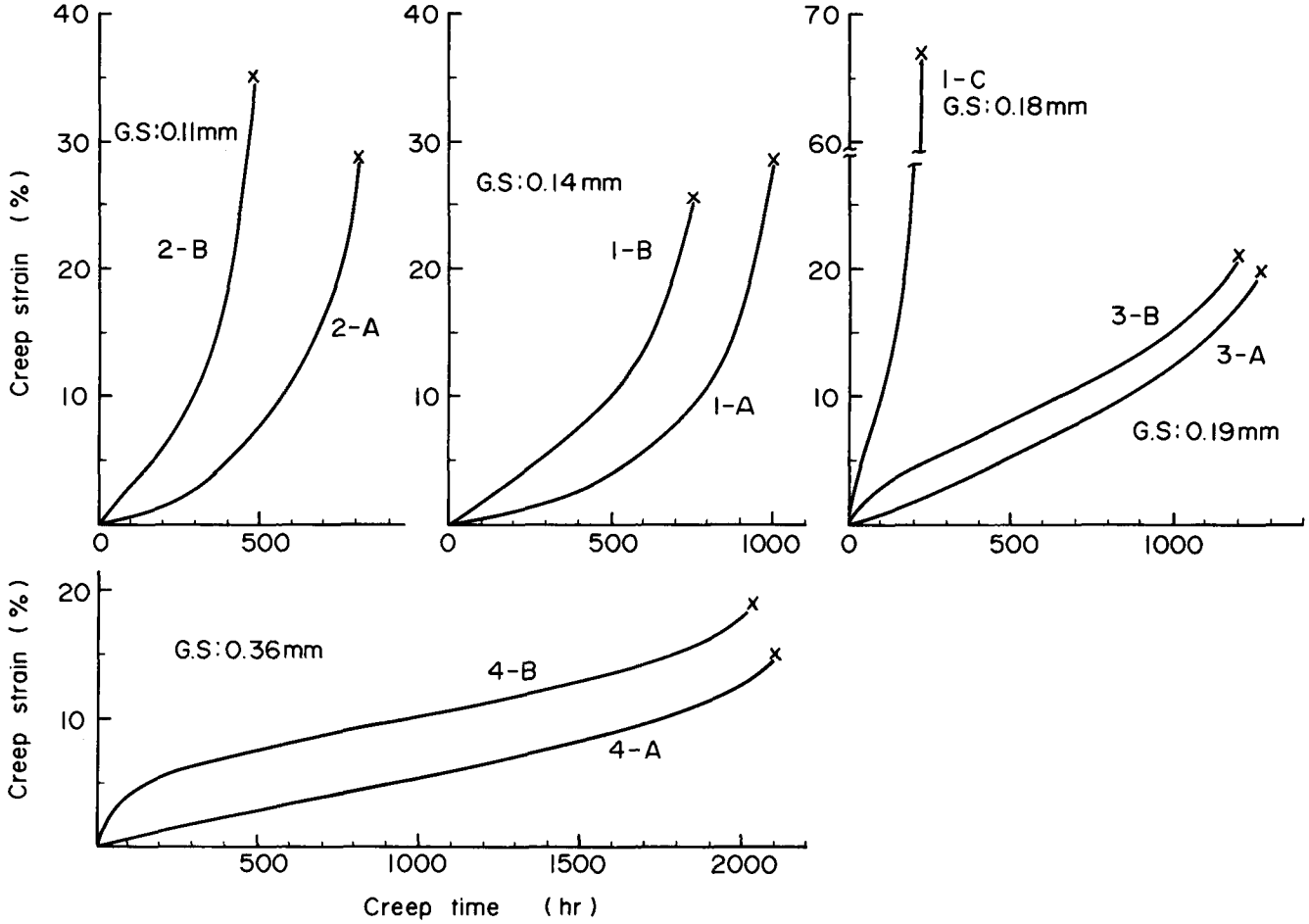

Fig. 5—Creep curves for nine samples tested at 1000 °C under a stress of 24.5 MPa (2.5 kg/mm²), G.S.: Grain size.

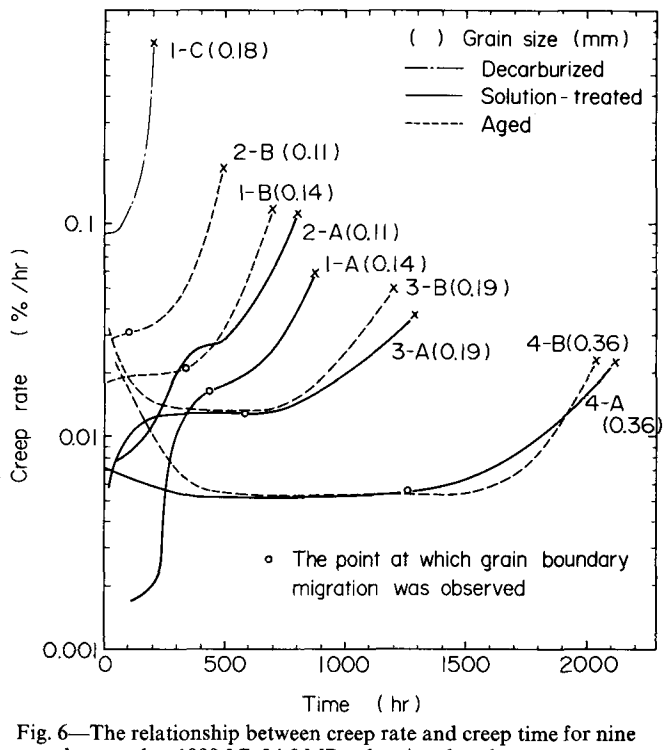

Fig. 6—The relationship between creep rate and creep time for nine samples tested at 1000 °C, 24.5 MPa, showing that the creep curves are influenced by prior heat treatment.

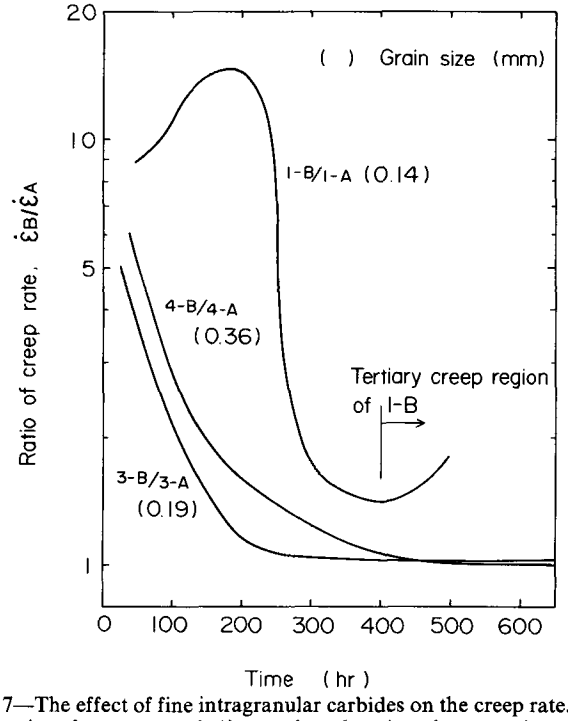

Fig. 7—The effect of fine intragranular carbides on the creep rate. The ratios of creep rates, $\dot{\epsilon}_B/\dot{\epsilon}_A$ are plotted against the creep times for each pair of the same grain size samples. $\dot{\epsilon}_A$ is the creep rate for the "A" series sample which was solution treated and $\dot{\epsilon}_B$ is that for the "B" series sample which was aged.

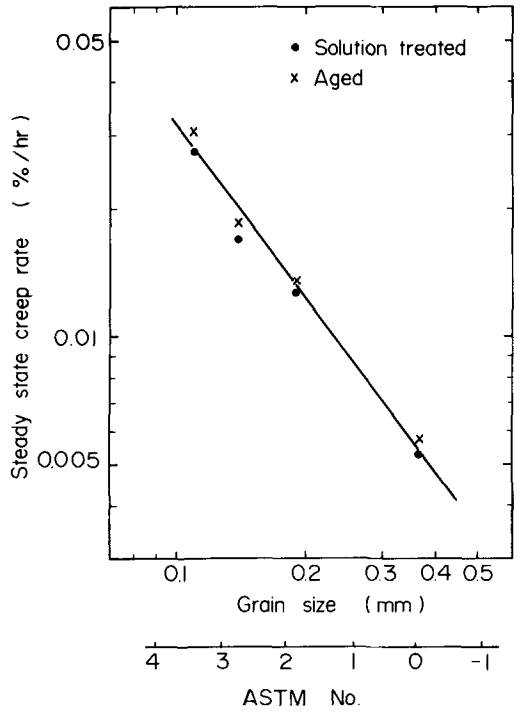

Fig. 8—The grain size dependence of the steady state creep rate at 1000 °C, 24.5 MPa. This finding shows that the steady state creep rate depends more on the grain size than on the heat treatment *per se*.

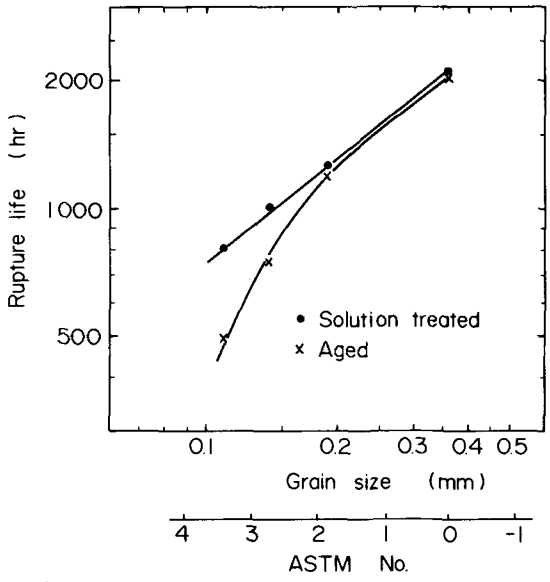

Fig. 9—The grain size dependence of the creep rupture life at 1000 °C, 24.5 MPa shows that the creep rupture lives for the smaller grain size samples are remarkably affected by the prior heat treatment conditions.

sive boundary, the diffusion of atoms forming the carbides from the compressive boundary region to the tensile boundary region and the reprecipitation of carbides on the tensile boundary.

Figure 13 shows an EPMA of carbides at a tensile boundary in specimen 1-A creep-ruptured at 1000 °C, 24.5 MPa after 1004 h. The thin and bright particle sandwiched between the dark particles is an M_6C type carbide; the dark particles are $M_{23}C_6$ type carbides. The M_6C type carbide is very rare on the tensile boundaries. The microstructures in Fig. 4 and 13 show that $M_{23}C_6$ type carbides form more readily on tensile boundaries during creep than they do on the stress-free boundaries during unstressed aging.

Although the migration of carbides and grain boundary migration occurred in all the samples, the times to achieve the microstructure shown in specimen 2-B were longer in other samples than in 2-B. Figure 14 shows the migration of carbides and the boundary migration at compressive boundaries that was observed in specimens 1-A, 3-A and 4-A. The aging times at which these microstructures were observed were 383, 720 and 1250 h for specimens 1-A, 3-A and 4-A, respectively. This suggests the grain size dependence of this phenomenon, *i.e.* the larger the grain size of the sample, the longer time is taken to achieve such a microstructure. The circles marked on the creep curves in Fig. 6 indicate the points at which the migration of carbides and grain boundary migration on compressive boundaries were clearly confirmed by an optical microscope of less than 500 magnification. Notice that the creep rates of all the samples gradually increase from those points. This result and the rapid occurrence of grain boundary migration in the carbide free specimen 1-C support the idea of Mino *et al.*[8] These authors propose that grain

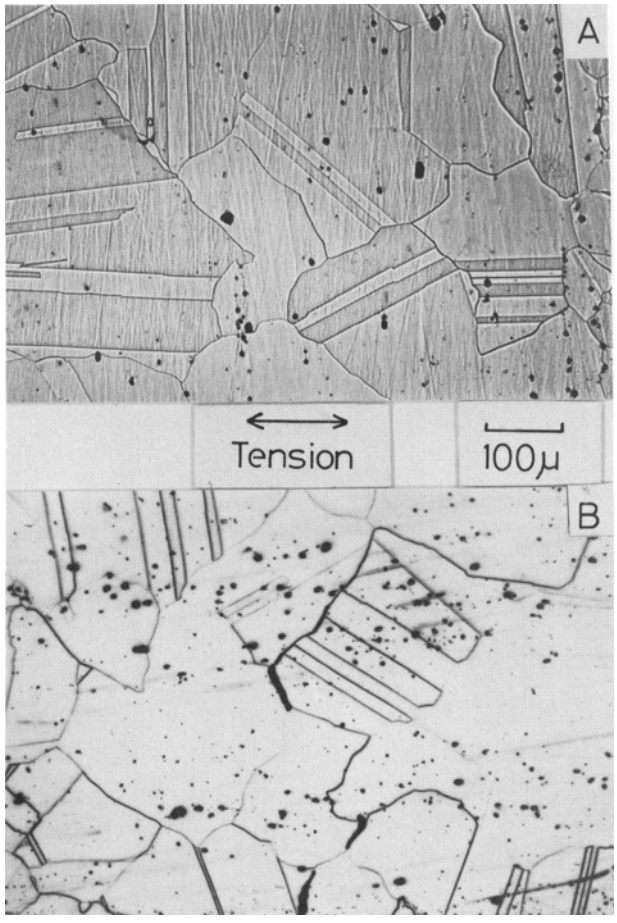

Fig. 10—The microstructural changes occurring in the carbide-free specimen 1-C (decarburized) during creep at 1000 °C under tensile stress of 24.5 MPa show A) wavy grain boundaries caused by grain boundary migration in the sample creep tested for 8 h to a strain of 2 pct and B) creep cracks initiated at some grain boundaries in the sample creep tested for 50 h to a strain of 10 pct.

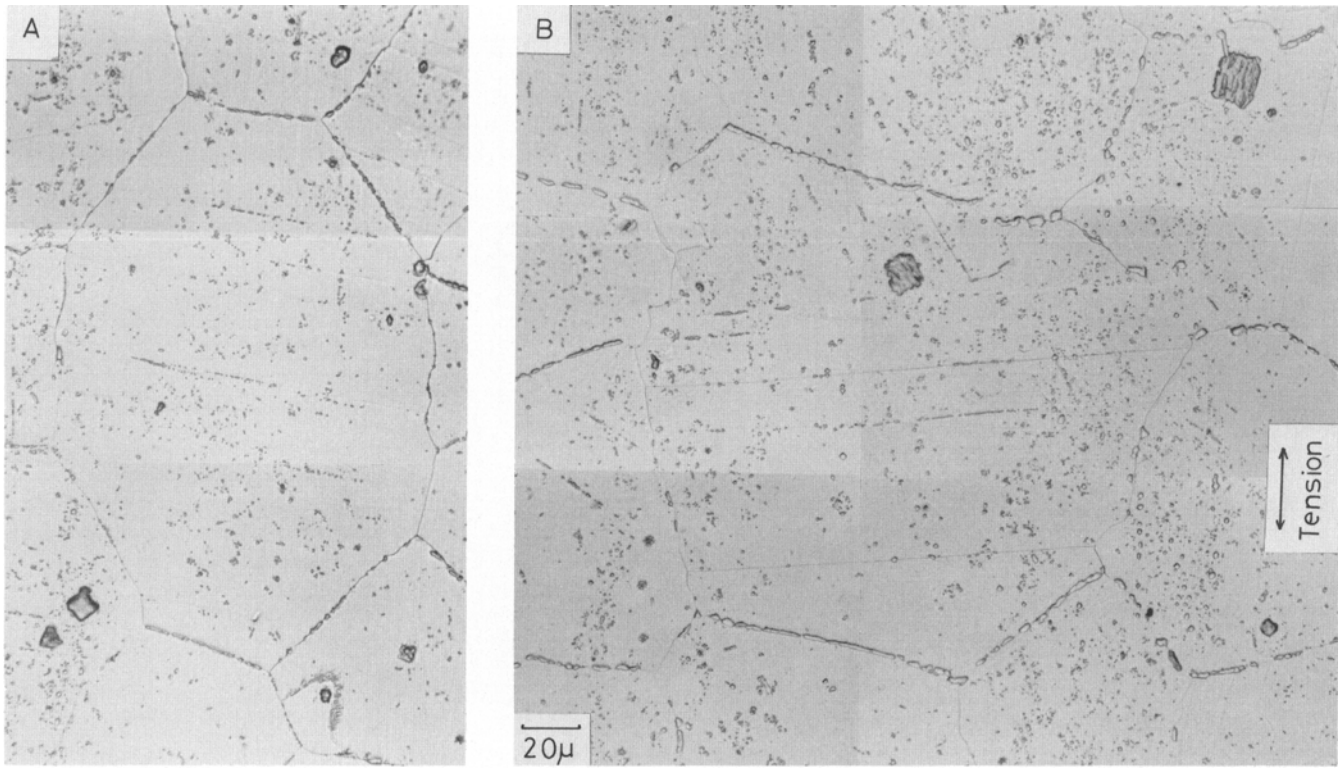

Fig. 11—The microstructural changes of specimen 2-B during tensile creep at 1000 ° C and 24.5 MPa, show preferred formation of carbides on grain boundaries which are perpendicular to the tensile stress axis and dissolution of carbides as well as grain boundary migration on grain boundaries which are parallel to the tensile stress axis. These specimens were creep tested for (*a*) 100 h to a strain of 2 pct and (*b*) 338 h to a strain of 4 pct, respectively.

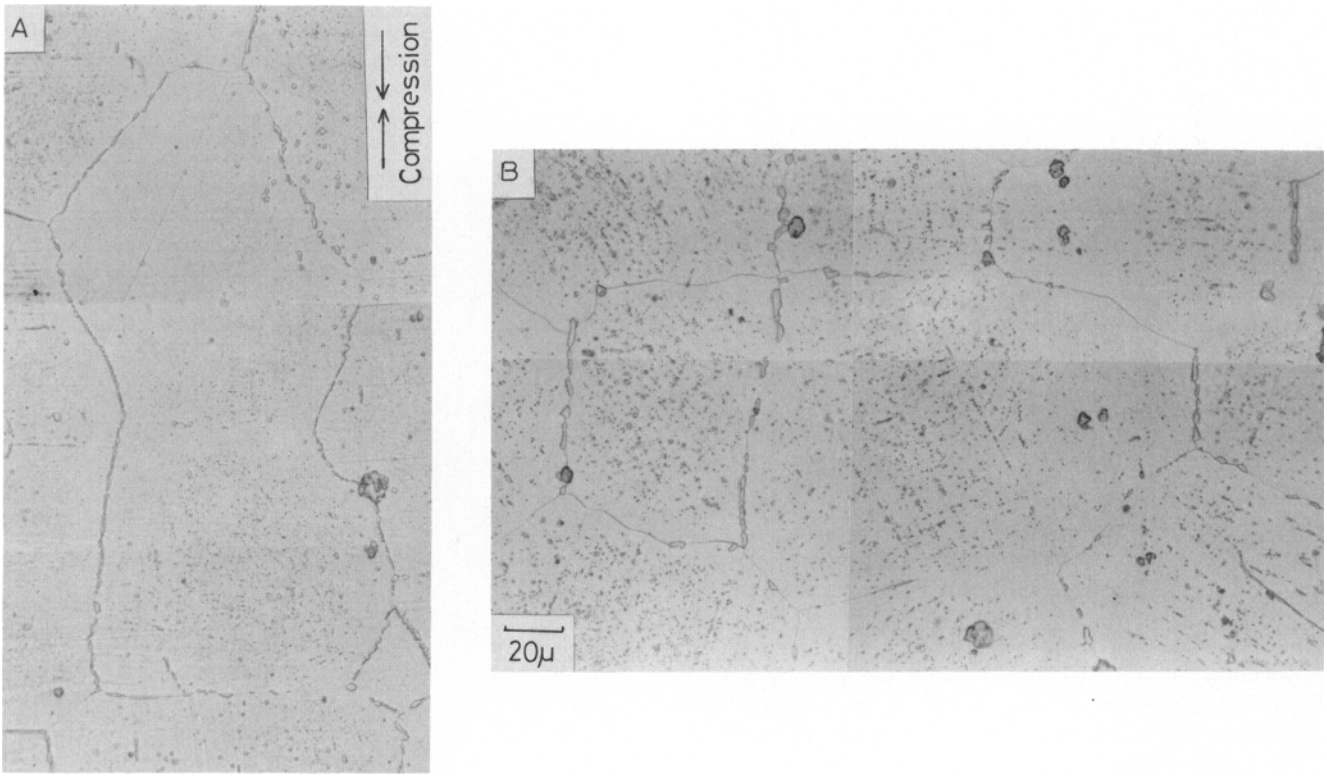

Fig. 12—The microstructural changes occurring in specimen 2-B during compressive creep at 1000 °C under a stress of 24.5 MPa, show preferred formation of carbides on grain boundaries which are parallel to the compressive stress axis and dissolution of carbide and grain boundary migration on grain boundaries which are perpendicular to the compressive stress axis. These specimens were creep tested for (*a*) 100 h and (*b*) 338 h, respectively.

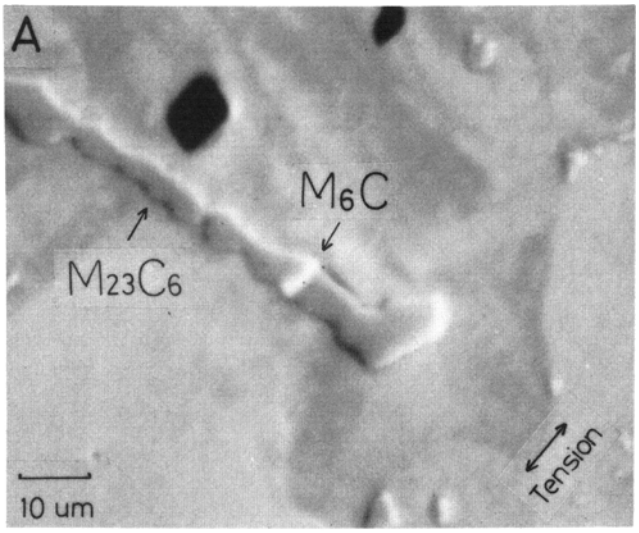

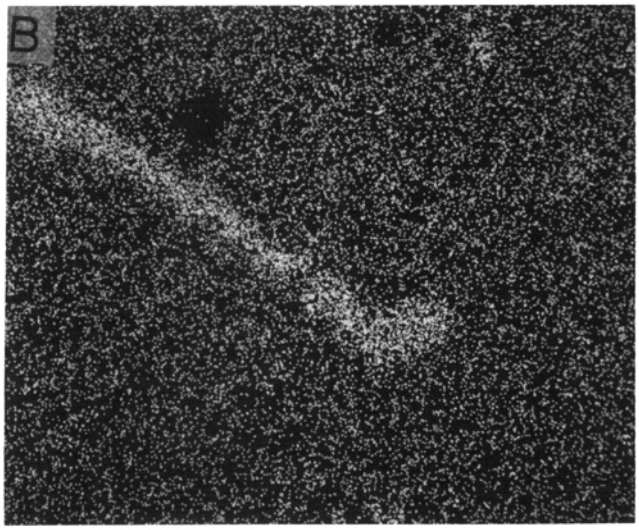

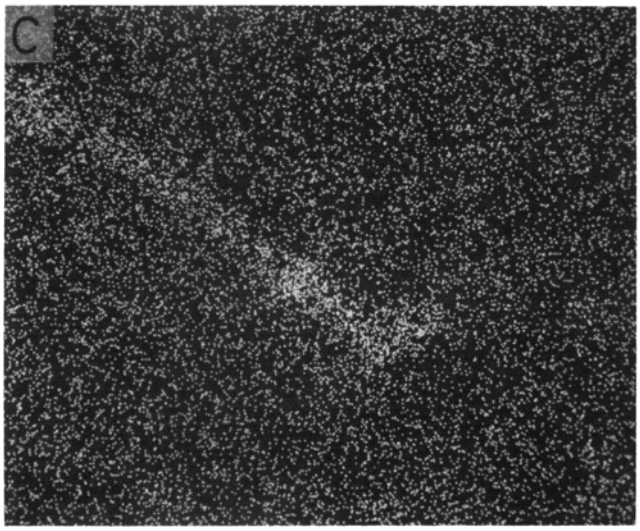

Fig. 13—Elemental X-ray images for grain boundary carbides at a tensile boundary of specimen 1-A creep-ruptured at 1000 °C, 24.5 MPa after 1004 h. (*a*) Backscattered electron image, (*b*) Cr-Kα and (*c*) Mo-Kα. It shows the existence of few M_6C type carbides and abundant $M_{23}C_6$ type carbides on the tensile boundary.

boundary carbides contribute to creep strength by suppressing grain boundary migration which is one of the recovery mechanisms.

An EPMA was made of chromium, nickel, molybdenum and cobalt concentration in the carbide-free

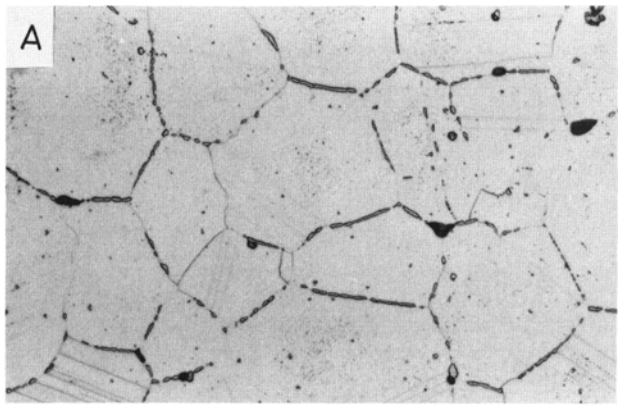

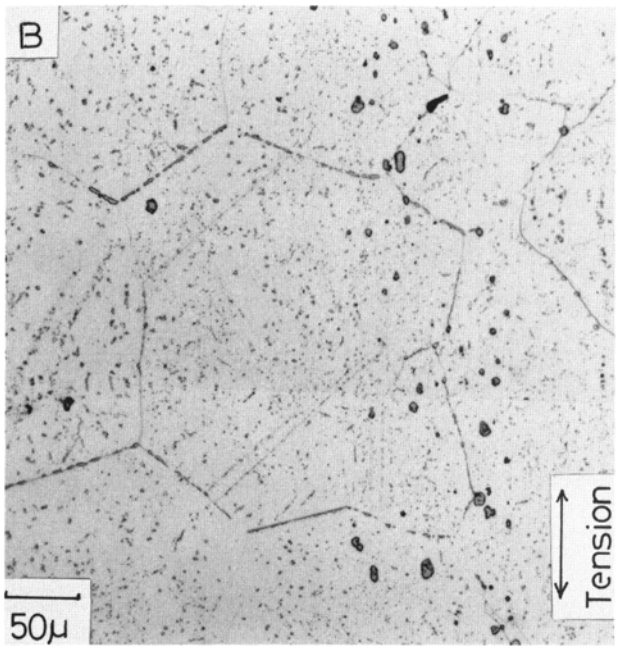

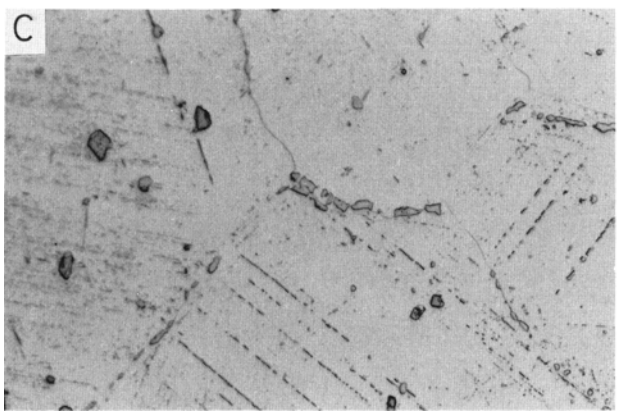

Fig. 14—Migration of grain boundary carbides and grain boundary migrations were observed in samples having various grain sizes (G.S). (*a*) Specimen 1-A (G.S: 0.14 mm) crept for 383 h to a strain of 4 pct, (*b*) 3-A (G.S: 0.17 mm) crept for 570 h to a strain of 4 pct and (*c*) 4-A (G.S: 0.36 mm) crept for 1275 h to a strain of 6.5 pct.

specimen 1-C creep-ruptured at 1000 °C, 24.5 MPa after 210 h. No mass transport of any of these atoms between the tensile boundary region and the compressive boundary region was observed. This indicates that carbon and/or carbides play the most important roles for the mass transport which occurred in all the undecarburized samples.

3.3 Discussion of the Mechanism of Grain Boundary Carbide Migration. The fact that no mass transport was observed in the carbide-free specimen 1-C suggests that it is the difference of stability of carbides between the compressive and the tensile boundaries which leads to the apparent migration of grain boundary carbides. Several possible mechanisms may explain the difference of stability of carbides between the compressive and the tensile boundaries.

The first candidate mechanism is concerned with the difference of equilibrium concentration of solute at the interface of carbide and matrix under stress. The relationship between the chemical potential μ_x of a solute x and the pressure P will be given[12,13]

$$\mu_x = \mu_0 + P\Omega \qquad [1]$$

where μ_0 is the chemical potential for the pressure free state and Ω is the atomic volume of solute x. In this case the chromium, molybdenum and carbon are taken into account as the solute. Equation [2] is derived from Eq. [1]

$$C = C_0\left(1 + \frac{P\Omega}{kT}\right) \qquad [2]$$

where C is the solute concentration in a particle, in equilibrium with a matrix, under pressure P; C_0 is that for the pressure free state and kT has its usual meaning. The pressure P at the interface of carbide and matrix is divided into two terms, the surface tension and the external stress terms. Thus Eq. [2] is rewritten as follows.

$$C = C_0\left[1 + \frac{\Omega}{kT}(\gamma K + \sigma)\right] \qquad [3]$$

where γ is the interfacial energy, K is the curvature of the particle on the interface and σ is the external stress acting normal to the surface. Equation [3] indicates that the solute concentration is increased by the compressive stress (positive σ) and decreased by the tensile stress (negative σ). Consequently the carbide dissolves under compressive stress and precipitates under tensile stress so as to keep the equilibrium concentration of solute at the interface. Furthermore, Eq. [3] also suggests that when the difference in size of carbide is introduced between the two boundaries, the usual Ostwald ripening caused by the difference of the curvature will accelerate the migration of carbide.

The second candidate mechanism is concerned with the difference of creep deformation of carbide. The grain boundary carbides that were exposed by a deep etch are shown in the SEM photo of Fig. 15. The carbides are dendritically grown on the plane of a grain boundary as have been reported for some austenitic stainless steels,[14,15] *i.e.* the carbide particle is not a spheroid but a cylindroid. Therefore the mechanism[13,16] for the spheroidization of lamellar structures seems to be applicable for the explanation of the instability of grain boundary carbides. A cylindrical carbide located on the plane of a compressive boundary is compressed in the direction normal to the plane of the boundary, while it is elongated in the direction parallel to the plane of the boundary by the elongation of the grains located on both sides of the boundary as shown in Fig. 16. When subgrains are formed in the matrix with increasing creep deformation, curvatures are introduced in the carbides by the surface tension of subgrain boundaries as illustrated Fig. 16, *i.e.* the cylindrical carbides become uneven during creep. The uneveness progresses more rapidly on a compressive boundary than on the tensile boundary since mechanical necking occurs in the cylindrical carbides on the compressive boundary as a result of the elongation in the longitudinal direction. Following again Eqs. [2] and [3], the equilibrium solute concentration at the interface increases with increasing curvature of the particle. Therefore the difference of equilibrium concentration of solute at the interface between the compressive and the tensile boundaries arises as a result of creep deformation. But the clear necking of carbide on compressive boundaries has not been observed in any samples crept.

The third candidate mechanism is concerned with the lattice orientation relationship. The grain boundary migration observed on the compressive boundary might hasten the dissolution of grain boundary carbide by eliminating the preferred lattice orientation relationship between the carbide and the matrix as indicated for

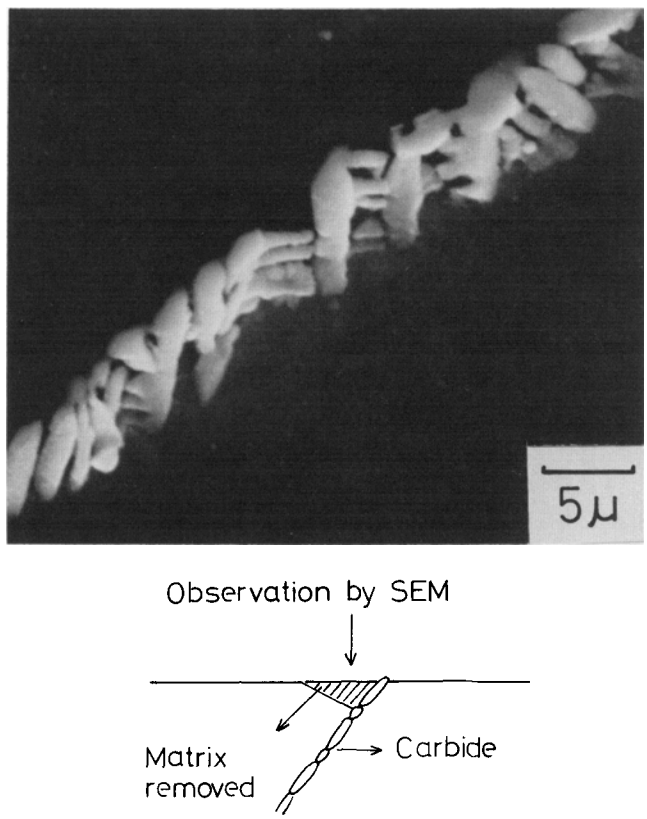

Fig. 15—Grain boundary carbides in specimen 1-A aged for 100 h at 1000 °C. The carbides were exposed by a deep etch and observed by SEM, showing a dendritic carbide growth on the grain boundary.

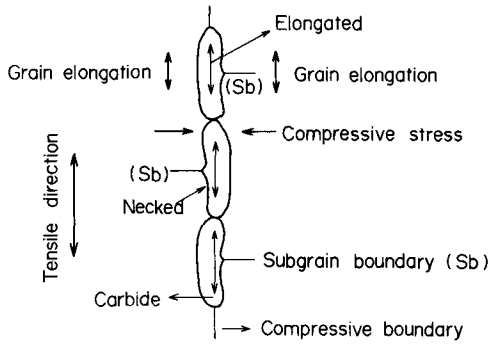

Fig. 16—Illustration for the morphological change of carbides on the compressive boundaries during tensile creep.

AISI type 304 stainless steel by Biss *et al.*[17]

All of the above three mechanisms support the difference of stability of carbides between the compressive and tensile boundaries. It is expected that the difference of stability of carbides is the main cause of the migration of grain boundary carbides.

In addition to these three mechanisms, Herring-Nabarro creep[18] is an applicable means to explain the mass transport which occurred in this alloy. Herring-Nabarro creep, which involves diffusion flux caused by differences in vacancy concentration near the tensile boundary and near the compressive boundary, has been reported for some nickel base alloys.[19,20]Tien and Gamble[20] suggested that Herring-Nabarro type mass transport was accomplished through the diffusion of chromium atoms which have the highest diffusion coefficient by the vacancy mechanism in a carbon-free Ni-16 Cr-5 Al-4 Ta alloy. Although Herring-Nabarro creep is not the controlling mode of creep in this alloy at 1000 °C, 24.5 MPa, this temperature is high enough that Herring-Nabarro creep does occur. Therefore it is expected that Herring-Nabarro creep assists the migration of carbides in this alloy.

The preferential precipitation of chromium rich $M_{23}C_6$ type carbide on the tensile boundary is understandable by the difference of diffusivity between chromium and molybdenum. Limited data[21] for the diffusivities of atoms in nickel base alloys show that the diffusion coefficient of chromium is higher than that of molybdenum. Therefore the chromium rich $M_{23}C_6$ type carbide is formed on the tensile boundary in preference to the molybdenum rich M_6C type carbide since chromium diffuses more rapidly than molybdenum.

The grain size dependence of grain boundary carbide migration is explainable by the fact that the diffusive fluxes of atoms and vacancies between the compressive and the tensile boundaries are proportional to the reciprocal of grain size.[22]

3.4 Microstructural Changes in Tertiary Creep Regions. Creep voids are initiated at the sites of grain boundary carbides on grain boundaries perpendicular to the tensile stress axis. Creep voids were observed in all samples crept to 4 pct elongation. Typical initiation sites of voids are shown in Fig. 17. Although voids are initiated at the site of grain boundary carbides, nevertheless samples containing grain boundary carbides have higher creep strength in general than do carbide-free samples (1-C). This is attributed to the effect of grain boundary carbides in suppressing creep deformation and in reducing the agglomeration of voids as observed in some austenitic cast steels.[23,24]

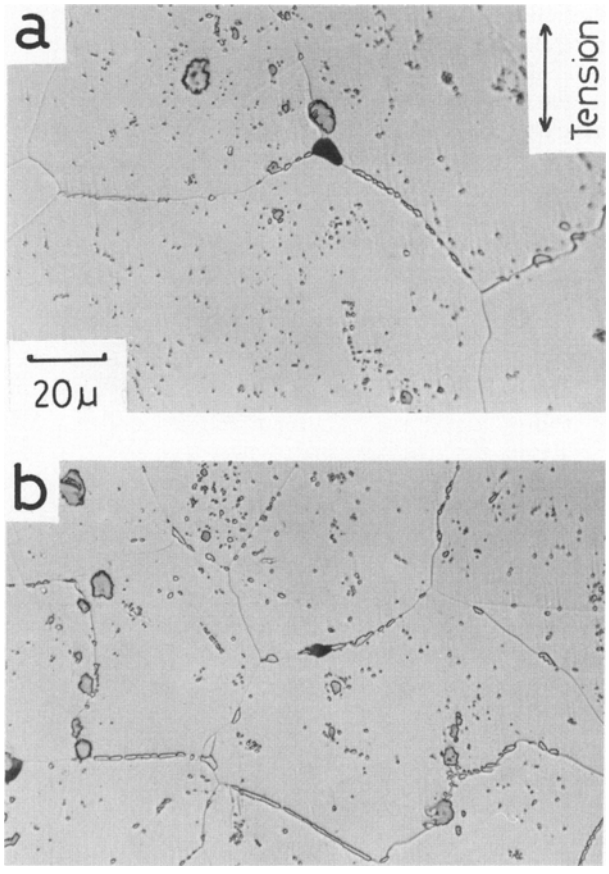

Fig. 17—Typical initiations of creep voids were observed in specimen 2-B which was creep tested for 200 h to a strain of 4 pct, (*a*) at a triple point of grain boundaries and (*b*) between discrete grain boundary carbide particles on a grain boundary perpendicular to the tensile stress axis.

Recrystallization also occurred in the tertiary creep regions of all samples crept. Figure 18 shows recrystallized grains in specimen 1-A which had been creep tested to rupture. The recrystallization accelerates creep deformation by breaking up the grains. Creep cracks are also initiated on carbide-free grain-boundaries which were formed by recrystallization.

CONCLUSIONS

The creep deformation and the microstructural changes of solution-treated Inconel 617 at 1000 °C progress as illustrated in Fig. 19. Correlating the creep deformation with the microstructural change, the following conclusions were obtained:

1) There is no precipitation in the sample fully solution-treated at 1200 °C for 20 h. The chromium rich $M_{23}C_6$ type carbide and the molybdenum rich M_6C type carbide rapidly precipitate on grain boundaries and as intragranular particles. (Step 1) This precipitation is so rapid that step 1 is achieved during short time preheating prior to loading for the creep test.

2) The unstable intragranular carbides redissolve in favor of the more stable grain boundary carbides. Thus the grain boundary carbides grow and the intragranular carbides disappear. (Step 2) The fine intragranular

carbides contribute to the creep strength in the early stages of the creep regime (within 300 h).

3) The grain boundary carbides migrate from grain boundaries that are under compressive stress to those that are under tensile stress. (Step 3) The migration of carbides is understandable in terms of a sequence in which thermodynamically and mechanically unstable carbides on compressive boundaries dissolve and the solute atoms forming the carbides diffuse from the compressive boundary region to the tensile boundary region, followed by the precipitation and growth of carbides at tensile boundaries. The rate of migration is inversely proportional to the grain size. This grain size dependence is due to the grain size dependence of the diffusive flux of atoms and vacancies between the two grain boundary regions.

4) When carbide precipitation occurs at tensile boundaries the $M_{23}C_6$ type carbide, having high chromium content, is preferentially formed. This is attributed to the higher diffusivity of chromium over that of molybdenum in nickel base alloys.

5) The potency of intragranular carbides in reducing creep rate decreases as creep progresses. Consequently the steady state creep rate depends not so much upon the initial carbide morphology as upon the grain size.

6) When the population of carbides becomes low enough at compressive boundaries, as a result of grain boundary carbide migration, that grain boundary starts to migrate. (Step 4) The creep rate then gradually increases with the occurrence of grain boundary migration which starts in the steady state region. This suggests that grain boundary carbides contribute to the reduction of the creep rate by suppressing grain boundary migration which is one of the recovery mechanisms.

7) Creep voids are initiated at carbides which reside on grain boundaries that are perpendicular to the tensile axis during steady state creep. (Step 4)

8) Recrystallization occurs as creep deformation progresses. (Step 5) The recrystallization accelerates creep deformation by breaking up the grains.

9) It is expected that the fine intragranular carbides contribute to the prolongation of creep rupture life in the lower temperature and high stress region, and that the grain size affects the creep rupture life in the higher temperature and lower stress region.

10) The grain size, the precipitation of fine intragranular carbide and the stability of grain boundary carbides should all be taken into account when estimating the long-term creep strength of this alloy.

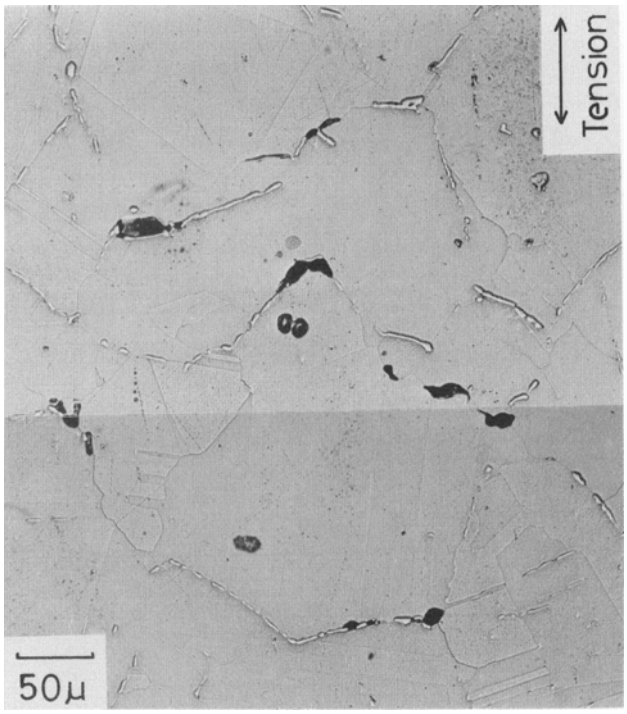

Fig. 18—The microstructure of specimen 1-A, which was creep tested to rupture, shows recrystallized grains, creep cracks, and migrated grain boundaries moving away from the coarsened carbides.

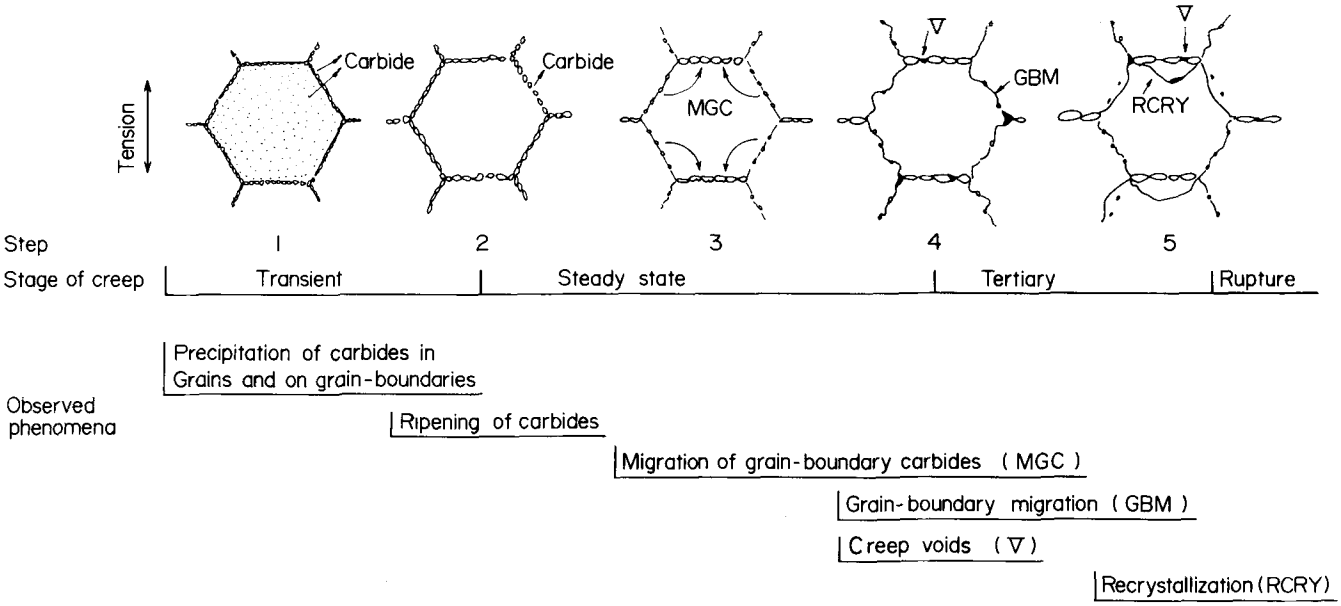

Fig. 19—A schematic representation of microstructural changes observed in solution treated Inconel 617 during creep at 1000 °C.

ACKNOWLEDGMENT

The authors gratefully acknowledge Mr. D. J. Tillack, Huntington Alloys, Inc., for furnishing the samples, Mr. T. Takahashi, National Research Institute for Metals, for supplying some useful information for the chemical analysis of the carbides and Dr. Y. G. Nakagawa and Mr. K. Mino, for discussing the stability of carbides under stress.

This work was supported in part by a research grant from the Materials Branch of the U.S. National Science Foundation and partly by a grant from Ishikawajima-Harima Heavy Industries Co., Ltd., Japan.

REFERENCES

1. National Project News 1976, published by the Ministry of International Trade and Industry of Japan, Tokyo, Japan.
2. R. L. Ammon and R. W. Buckman: *Trans. ANS.*, 1977, vol. 26, p. 202.
3. R. K. Bhargava, J. Moteff, and R. W. Swindeman: *Met. Trans. A*, 1976, vol. 7A, p. 879.
4. W. L. Mankins, J. C. Hosier, and T. H. Bassford: *Met. Trans.*, 1974, vol. 5, p. 2579.
5. T. Takahashi, J. Fujiwara, T. Matsushima, M. Kiyokawa, I. Morimoto, and T. Watanabe: *Trans. Iron Steel Inst. Jpn.*, 1978, vol. 18, p. 221.
6. Y. Hosoi and S. Abe: *Met. Trans. A*, 1975, vol. 6A, p. 1171.
7. Y. Saiga, A. Ohtomo, and K. Mino: Report of the 123rd Committee on Heat-Resisting Metals and Alloys, Japan Society for the Promotion of Science, 1974, vol. 15, p. 155.
8. K. Mino and A. Ohtomo: *Trans. Iron Steel Inst. Jpn.*, 1978, vol. 18, p.731.
9. T. Takahashi: Private communication, National Research Institute for Metals, Tokyo, Japan.
10. F. Garofalo: *Fundamentals of Creep and Creep-rupture in Metals*, p. 146, The Macmillan Company, New York, 1965.
11. F. Garofalo, R. W. Whitmore, W. F. Domis, and F. von Gennigen: *Trans. TMS—AIME*, 1961, vol. 221, p. 310.
12. R. Raj. and M. F. Ashby: *Met. Trans.*, 1971, vol. 2, p. 1113.
13. Y. G. Nakagawa and G. C. Weatherly: *Met. Trans.*, 1972, vol. 3, p. 3223.
14. F. G. Wilson: *J. Iron Steel Inst.*, 1971, vol. 209, p. 126.
15. M. Yamazaki, T. Arai, and Y. Koizumi: Report of the 123rd Committee on Heat-Resisting Metals and Alloys, Japan Society for the Promotion of Science, 1973, vol. 14, p. 69.
16. C. D. Himmelblau and N. J. Grant: *Conference on in situ composites II*, p. 505, Xerox Individualized Publishing, Lexington, MA, 1976.
17. V. Biss, D. L. Sponseller, and M. Semchyshen: *J. Mater.*, 1972, vol. 7, p. 88.
18. C. Herring: *J. Appl. Phys.*, 1950, vol. 21, p. 437.
19. T. B. Gibbons: *Met. Sci. J.*, 1972, vol. 6, p. 13.
20. J. K. Tien and R. P. Gamble: *Met. Trans.*, 1971, vol. 2, p. 1663.
21. A. Davin, V. Leroy, D. Coutsourads, and L. Habraken: *Memories Scientifiques Rev. Metallurg*, 1963, vol. 60, p. 275.
22. B. Barton: *Diffusional Creep of Polycrystalline Materials*, p. 2, Trans Tech Publications, Bay Village, OH, 1977.
23. S. Kihara, K. Asakawa, A. Ohtomo, and Y. Saiga: Ishikawajima-Harima Heavy Industries Engineering Review, 1975, vol. 8, p. 17.
24. T. Shinoda, M. B. Zaghloul, Y. Kondo, and R. Tanaka: *Trans. Iron Steel Inst. Jpn.*, 1978, vol. 18, p. 139.